Sensors and Materials, Vol. 38, No. 6 (2026) 3077–3088
MYU Tokyo

S & M 4490

Development of Data-driven Virtual Sensor Framework for Real-time Property Prediction in Intelligent Heat Treatment Systems

Te-Kang Tsao*

Department of Mechanical Engineering, National Kaohsiung University of Science and Technology,
No. 415, Jiangong Rd., Sanmin Dist., Kaohsiung 807618, Taiwan (R.O.C.)

(Received February 10, 2026; accepted April 6, 2026)

Keywords: virtual sensor, heat treatment monitoring, hardenability, microstructure evolution, data-enabled materials

In intelligent manufacturing environments, the real-time awareness of material properties during heat treatment is essential for ensuring both product reliability and process stability. However, key internal states such as phase evolution and mechanical performance cannot be directly accessed using conventional physical sensors. In this study, a data-driven virtual sensor framework is developed for SAE 1038 medium-carbon steel to enable the nondestructive, real-time estimation of mechanical properties. Unlike conventional static regression models, the proposed framework incorporates the ideal critical diameter (D_I) as a material descriptor to enable the adaptive normalization of batch-to-batch chemical variations. The virtual sensor integrates a comprehensive heat treatment database established through high-resolution dilatometry, Jominy end-quench testing, and mass effect analyses across multiple specimen diameters. Metallographic observations and SEM fractography are employed to validate the correspondence between predicted properties and underlying microstructural evolution. By coupling D_I and tempering temperature into the proposed sensing logic, hardness and ultimate tensile strength are predicted with maximum errors of less than 5%. Furthermore, fracture morphology analysis reveals a systematic transition from quasi-cleavage to microvoid coalescence with increasing tempering temperature, providing a microstructural basis for defining the safe operating regime of self-sensing fasteners. The proposed virtual sensing framework demonstrates a practical and scalable approach for transforming conventional structural steels into data-enabled materials, offering a viable pathway toward real-time quality assurance and integration into intelligent heat treatment systems.

1. Introduction

In modern intelligent manufacturing systems, the ability to sense and control material states during processing has become a critical requirement for achieving consistent product quality and operational reliability. While physical sensors are widely deployed to monitor environmental

*Corresponding author: e-mail: tktsao@nkust.edu.tw
https://doi.org/10.18494/SAM6285

ISSN 0914-4935
https://myukk.org/

parameters such as temperature, time, and atmosphere in heat treatment processes, they remain incapable of directly capturing internal material states, including phase evolution, mechanical properties, and failure susceptibility. This limitation creates a critical information gap between process control and material performance. To address this challenge, virtual sensing has emerged as an integrated estimation architecture rather than a standalone regression equation. In this study, the proposed virtual sensor combines (a) multisource physical inputs, including dilatometric transformation data, hardenability characterization, and mass effect behavior; (b) physically interpretable descriptors such as the ideal critical diameter (D_I); and (c) regression-based predictive functions structured for online deployment. Within this context, medium-carbon steel SAE 1038 used in high-strength fasteners represents an ideal platform for virtual sensor development, as its functional performance is highly sensitive to heat treatment history and microstructural evolution.[1–3] For instance, by utilizing the piezomagnetic effect, where mechanical stress induces measurable changes in magnetic permeability,[4–6] bolts manufactured from SAE 1038 can function as integrated sensors for real-time structural health monitoring. However, the functional reliability of such self-sensing components is highly sensitive to their internal microstructural state. The precision and signal-to-noise ratio of the sensing signal are directly dictated by the phase constituents. That is, an inconsistent heat treatment can lead to nonuniform magnetic domain wall pinning, causing erratic sensing data.[7–10] Furthermore, the fracture toughness and failure mechanisms define the operational limits of these smart sensors. A sudden brittle failure without prior microdeformation could lead to catastrophic sensor loss in critical infrastructure. As a result, establishing a reliable virtual sensing framework for such materials can be essential for advancing sensor-integrated manufacturing and realizing data-enabled structural components.

Despite these critical factors, traditional heat treatment monitoring relies on external environmental parameters (e.g., furnace temperature), which fail to "sense" internal metallurgical evolution. While various hardness prediction models have been proposed to optimize heat treatment parameters, most previous studies have focused on specific alloy compositions or small-scale laboratory specimens.[11–14] These conventional regression-based models often neglect the inherent batch-to-batch chemical variations and the complex mass effects encountered in industrial components. Consequently, such static models lack the flexibility required for real-time process adaptation when the material's hardenability fluctuates. To improve upon these limitations, the present work utilizes D_I as a fundamental normalizing parameter within the virtual sensing framework. Unlike previous tempering models calibrated for fixed compositions, the introduction of D_I enables adaptive normalization across different material heats. By integrating this descriptor with cooling capacity and tempering temperature, the framework can more accurately reflect the physical reality of the material's microstate, ensuring both structural integrity and sensing reliability.

Building upon the aforementioned virtual sensing architecture, in this work, the framework is systematically validated for SAE 1038 steel. The development of this sensing logic is based on several fundamental metallurgical assumptions: (a) the attainment of a predominantly martensitic state (> 90%) after quenching to ensure a consistent starting microstructure, (b) an isothermal tempering process that reaches metallurgical equilibrium, and (c) chemical compositions remaining within the standard SAE 1038 specifications. These boundaries

explicitly define the applicable metallurgical domain of the proposed virtual sensor. To demonstrate the real-time utility of the framework, a conceptual integration scenario is provided where the virtual sensor operates within an intelligent furnace control loop. By bridging the information gap between microscopic phase evolution and macroscopic mechanical performance, this work offers a practical and scalable pathway for the deployment of self-sensing structural components in smart manufacturing environments.

2. Experimental Procedures

2.1 Material characterization and sensing setup

As-received SAE 1038 steel wire rods were utilized in this study. To account for chemical variations in industrial production, two levels of carbon (0.35 and 0.40 wt%) and manganese (0.70 and 0.87 wt%) within the standard specification were analyzed. The primary chemical compositions, verified by optical emission spectroscopy (OES), are listed in Table 1.

2.2 Dilatometric analysis

To provide high-fidelity inputs for the virtual sensor, phase transformation temperatures were measured using a high-resolution dilatometer (DIL 805A). Cylindrical specimens (ø3 mm × 10 mm) were heated to 860 °C at a rate of 5 °C/s and subsequently cooled at various rates up to 10 °C/s. The dimensional changes recorded by the dilatometer's linear variable differential transformer (LVDT) were used to determine the Ac_1 and Ac_3 points, which are critical for the virtual sensor's logic.

2.3 Hardenability and mass effect sensing

Standard Jominy end-quench tests were conducted to establish the baseline hardenability curve.[15] Furthermore, to simulate the three-dimensional heat transfer in actual fasteners, mass effect measurements were performed. Cylindrical bars (100 mm in length) with diameters of 5, 10, 15, and 20 mm were sectioned at their midpoints. Microhardness (Hv) values were then measured along the radial direction from the core to the surface to quantify the impact of specimen geometry on cooling performance.[16]

2.4 Heat treatment database and metallographic characterization

For heat treatment, the specimens were subjected to oil quenching followed by tempering (Q&T) from 200 to 600 °C for 2 h. To correlate the virtual sensor's predictions with physical

Table 1
Chemical compositions of as-received SAE 1038 (unit: wt%).

	C	Si	Mn	P	S
High C, Mn	0.40	0.23	0.87	0.01	0.01
Low C, Mn	0.35	0.22	0.70	0.01	0.01

reality, extensive metallographic examinations were performed. Specimens were sectioned, mounted, and polished in accordance with standard protocols, concluding with a 1 μm alumina suspension. Microstructures were revealed using a 3% Nital etchant and observed by optical microscopy (OM; OLS 5100, Olympus) and SEM (Sigma 300 VP, Zeiss). Mechanical properties were quantified through Rockwell C (HRC) hardness tests[17] and uniaxial tensile tests.[18] Tensile testing was conducted on a universal testing machine at a constant crosshead speed of 2 mm/min to determine yield strength (σ_{Ys}), ultimate tensile strength (σ_{UTS}), and elongation (El). Then, the fracture surfaces of the tensile specimens were analyzed by SEM to identify failure mechanisms. Finally, hardness and tensile property predictions were developed in accordance with regression methods, constituting the core of virtual sensing.

3. Results and Discussion

3.1 Calibration of virtual sensor by dilatometry

To develop the virtual sensor model, the results of the dilatometric analysis are shown in Fig. 1. The critical temperatures for the low C, Mn variant were determined to be Ac_3 = 797 °C and Ac_1 = 780 °C. In comparison, the high C, Mn variant exhibited slightly lower thresholds, Ac_3 = 791 °C and Ac_1 = 778 °C. These precise thresholds allow further optimization of energy consumption by avoiding unnecessary overheating while ensuring full austenitization.

3.2 Mass effect analyses

Jominy end-quench tests results are shown in Fig. 2. With HRC 50 as the benchmark, high C SAE 1038 exhibits a hardening depth of about 5 mm, exceeding the 3 mm measured for the low C sample.

The mass effect results are shown in Fig. 3. It was found that the mass effect is primarily governed by the dimensions of the workpiece; as the diameter increases, the core becomes less

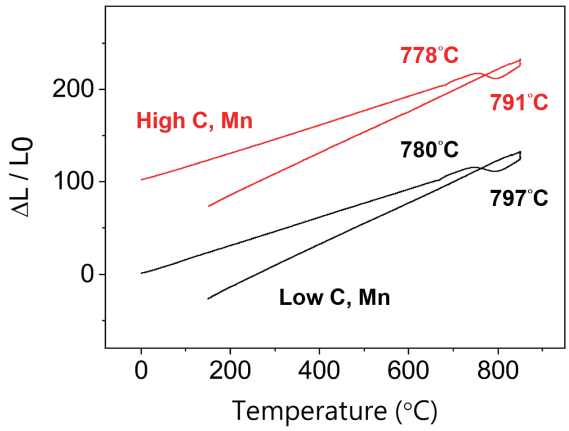

Fig. 1. (Color online) Results of dilatometric analysis of SAE 1038.

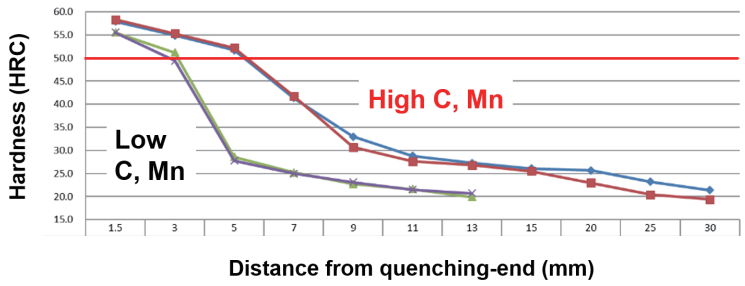

Fig. 2. (Color online) Jominy end-quench test results for SAE 1038.

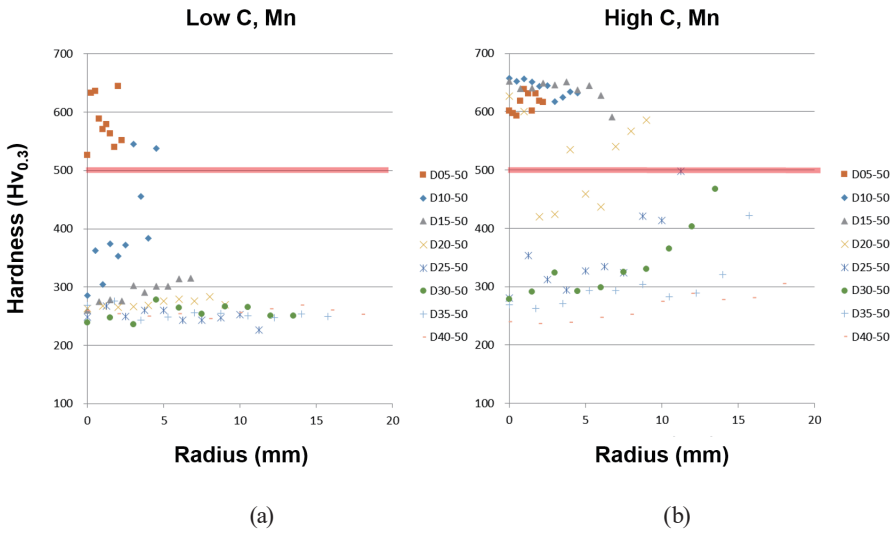

(a) (b)

Fig. 3. (Color online) Results of mass effect analyses of SAE 1038 with (a) low and (b) high C, Mn.

sensitive to quenching acceleration, leading to reduced hardness (mass effect), whereas sections closer to the quenched-end exhibit higher hardness. The steel with higher C content, characterized by superior hardenability, is less affected by the mass effect. In contrast, with lower C, Mn, when the diameter exceeds 10 mm, the hardness of both the surface and the core deteriorates significantly. Regarding bolt production, for components with a length of 100 mm and dimensions exceeding M5, SAE 1038 steel with high C and Mn content is more suitable owing to its superior hardenability, which is necessary to ensure consistent mechanical properties across larger cross sections. These observed microstructural gradients across different specimen diameters serve as the physical ground truth for the virtual sensor's training database.

3.3 Microstructural evolution

The virtual sensor's reliability is rooted in its ability to estimate phase fractions; therefore, microstructural evolution is critical. For the Jominy end-quench hardenability test, metallographic samples were prepared at the positions where hardness was measured along the side of the test bar. Figure 4(a) shows the microstructures of low C, Mn SAE 1038 at the

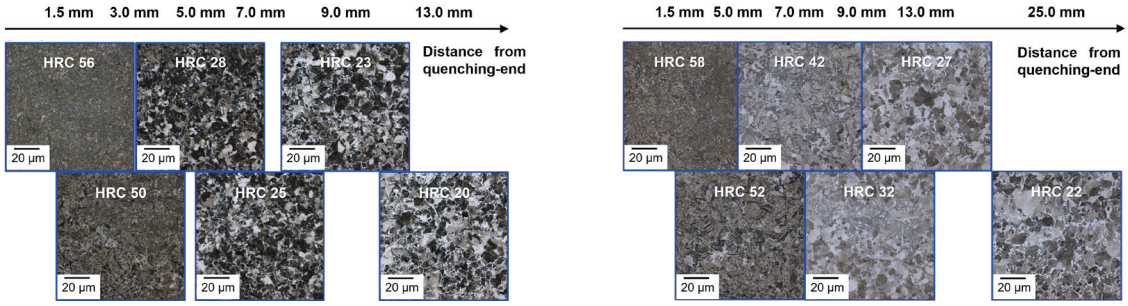

(a) (b)

Fig. 4. (Color online) Microstructure evolution of SAE 1038 with (a) low and (b) high C, Mn.

corresponding hardness locations. At the quenched end (1.5 mm from the edge), the hardness is HRC 56 and the corresponding microstructure is martensite. At the second point (HRC 50), partial bainite can be observed. The third point (HRC 28) consists of bainite along with pearlite and proeutectoid ferrite at the grain boundaries. Beyond 7 mm from the quenched end, the microstructure is predominantly pearlite; further from the quenched end, the more abundant and coarse microstructure is ferrite. The microstructures of the high C, Mn sample, which exhibits superior hardenability, are shown in Fig. 4(b). At the quenched end with the martensitic structure, the hardness HRC 58 is slightly higher. At further distances from the quenched end, the cooling rate decreases, leading to a gradual increase in the proportion of bainite. At approximately 9 mm from the quenched end, hardness drops to HRC 32, and the microstructure consists of bainite and pearlite. At a distance of 13 mm, where hardness is HRC 27, the structure reveals bainite and pearlite along with grain-boundary ferrite.

The hardenability test generated varying cooling rates in accordance with the distance from the quenched end. These results indicate that with a higher cooling rate, the nose of the ferrite or bainite transformation curves is bypassed, resulting in a predominantly martensitic structure. In contrast, lower cooling rates lead to the prior precipitation of ferrite or bainite, while even lower rates result in a mixture of ferrite, pearlite, and bainite. A clear transition from predominantly martensitic (HRC > 55) to predominantly bainitic structures (HRC 50–30) is observed in the measured hardness gradients, providing the necessary metallurgical basis for calibrating the virtual sensor framework.

For mass effect analysis, microstructures were observed at the midsection of a 100-mm-long bar. Figure 5 shows the microstructures of SAE 1038 with superior hardenability across diameters of 15, 20, and 25 mm. The core of the 15 mm bar remained predominantly martensitic, whereas increasing amounts of bainite and ferrite appeared in the 20 and 25 mm bars, respectively. Although quantitative phase analysis such as X-ray diffractometry can provide additional numerical precision, in medium-carbon steels, hardness evolution is widely accepted as a reliable indirect indicator of martensitic transformation. In this study, microstructural states identified by OM and SEM are consistent with D_I-based hardenability principles. Specifically, established hardness–martensite empirical correlations reported in hardenability literature (e.g.,

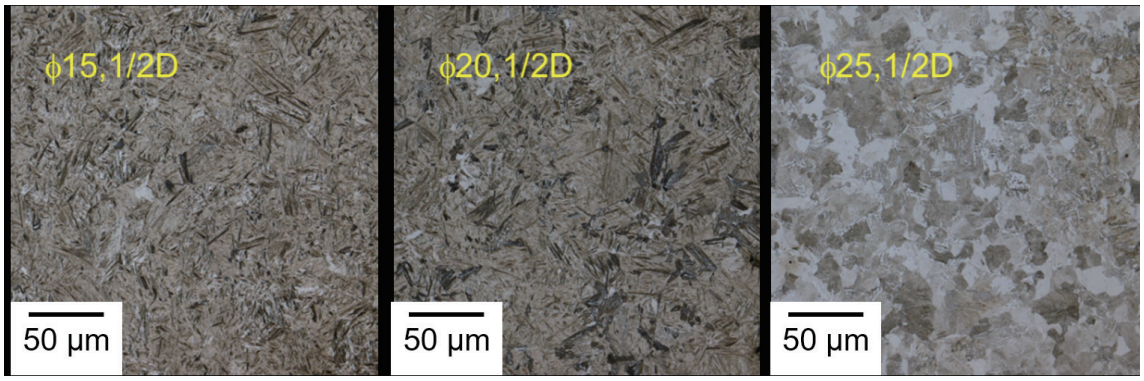

Fig. 5. (Color online) Microstructure evolution determined from mass effect analyses of SAE 1038 with high C, Mn.

HRC > 55 corresponding to predominantly martensitic structures) are employed to support the validation of the virtual sensing framework. As the diameter increased from 15 to 25 mm, the estimated martensitic content at the core decreased systematically, corresponding to the reductions in cooling rate and effective hardenability depth.

3.4 Mechanical performance and fracture morphology

For the mechanical performance after Q&T heat treatment processes, Table 2 systematically shows the hardness and tensile strength of SAE 1038 with high C, Mn (superior hardenability) along with various tempering conditions. After quenching, the hardness reached HRC 58 and gradually decreased to HRC 24 with further tempering to 600 ℃. In addition, a similar trend of ultimate tensile stress could be observed from 2163 to 846 MPa, while elongation significantly improved from 2.8 to 24.6%. These results demonstrate a strong correlation between the thermal history and the resulting mechanical performance.

SEM fractographs are shown in Fig. 6, providing clear evidence of the material's failure modes. The fracture surface of the quenched specimens exhibited quasi-cleavage features with minimal plastic deformation, indicating a high-strength but low-toughness condition. In contrast, the tempered specimens displayed a dense population of microvoid coalescence (dimples), confirming a ductile fracture mechanism. This transition from quasi-cleavage to microvoid coalescence reflects the change in mechanical stability under extreme loading conditions. Furthermore, incorporating these fracture characteristics into the virtual sensing framework may provide additional insight into potential failure behavior, which is relevant for the safety assessment of self-sensing fasteners.

To further clarify the relevance of fracture morphology to sensing reliability, sensing bolts operating under mechanical loading must maintain a stable elastoplastic response prior to failure. The observed transition from quasi-cleavage to microvoid coalescence with increasing tempering temperature corresponds to increased ductility and energy absorption capability. This transition reduces the likelihood of abrupt brittle failure, which could otherwise compromise

Table 2
Results of hardness and tensile tests for Q&T SAE 1038 with high C, Mn.

	as-Q	T200	T300	T400	T500	T600
Hardness (HRC)	58	50	47	41	32	24
σ_{Ys} (MPa)	1832	1603	1514	1238	893	728
σ_{UTS} (MPa)	2163	1918	1683	1348	1005	846
El (%)	2.8	4.0	6.8	9.3	18.4	24.6

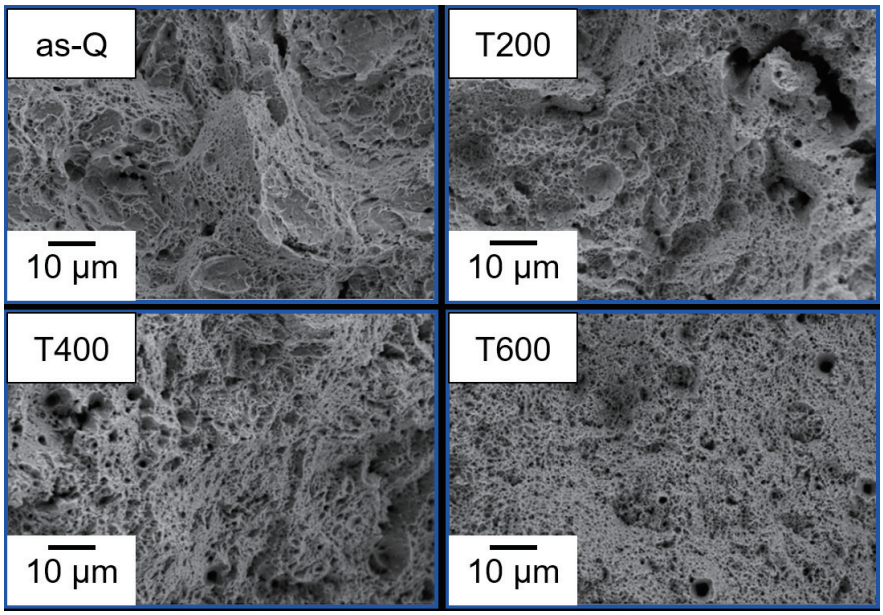

Fig. 6. (Color online) SEM fractography images of Q&T SAE 1038 after tensile tests.

sensing continuity in structural health monitoring applications. Therefore, fracture morphology serves as the microstructural validation of mechanical stability within the virtual sensing framework rather than being merely a descriptive metallographic observation.

3.5 Integration with intelligent manufacturing

The development of the virtual sensor logic is aimed at the transformation of discrete metallurgical data into a continuous property prediction framework for real-time estimation. Unlike conventional regression models that are often restricted to fixed chemical compositions, the proposed virtual sensor incorporates D_I[19–20] as a key normalizing parameter. This enables adaptation to batch-to-batch chemical variations within the SAE 1038 specification. By synthesizing the results of mass effect analysis and tempering experiments, two primary sensing equations were derived to estimate hardness (H) and ultimate tensile strength (UTS).

To ensure predictive fidelity, several underlying metallurgical assumptions are explicitly defined: (a) the target location within the component must achieve a predominantly martensitic state (>90%) during quenching, (b) the tempering process is assumed to be isothermal and of sufficient duration to reach metallurgical equilibrium, and (c) the chemical composition of the material must remain within the standard SAE 1038 grade limits. Under these conditions, the relationship between hardenability (D_I), tempering temperature (T), and the resulting mechanical properties can be mathematically formulated.

As illustrated in Fig. 7, a quadratic polynomial was employed to regress the hardness data. By interpolating the resulting coefficients against the D_I values, the governing equation for hardness prediction was established:

$$H(D_I, T) = (2.9776 \cdot D_I + 49.976) - (0.0121 \cdot D_I + 0.0171) \cdot T + (0.00003 \cdot D_I - 0.000129) \cdot T^2, \quad (1)$$

where $H(D_I, T)$ is the hardness function (predicted hardness value), D_I is the ideal critical diameter, and T is the tempering temperature (unit: °C).

A similar framework was applied to the UTS, as shown in Fig. 8, utilizing a cubic polynomial to capture the softening kinetics during tempering:

$$\begin{aligned} UTS(D_I, T) = {} & (626.53 \cdot D_I + 1169.3) + (0.4985 \cdot D_I - 0.0164) \cdot T \\ & + (-0.005781 \cdot D_I - 0.00186) \cdot T^2 + (0.000006 \cdot D_I) \cdot T^3, \end{aligned} \quad (2)$$

where $UTS(D_I, T)$ is the UTS function (MPa), D_I is also the ideal critical diameter, and T is the tempering temperature (unit: °C).

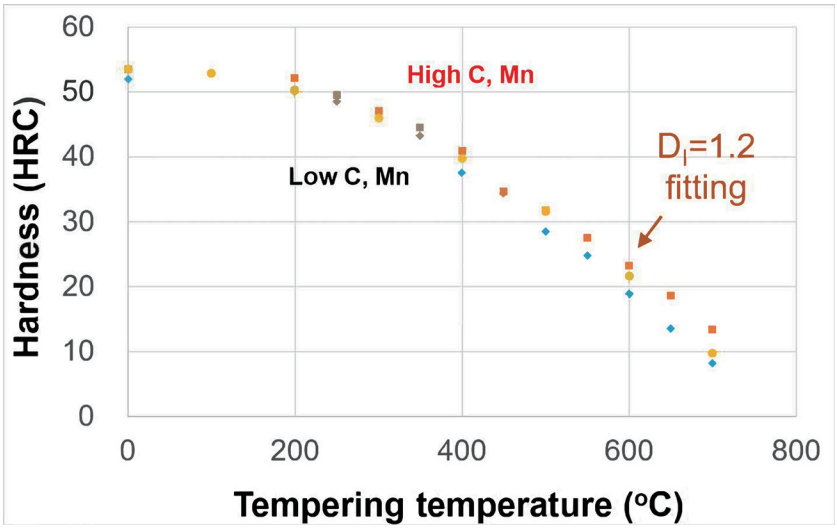

Fig. 7. (Color online) Hardness fitting model of Q&T SAE 1038.

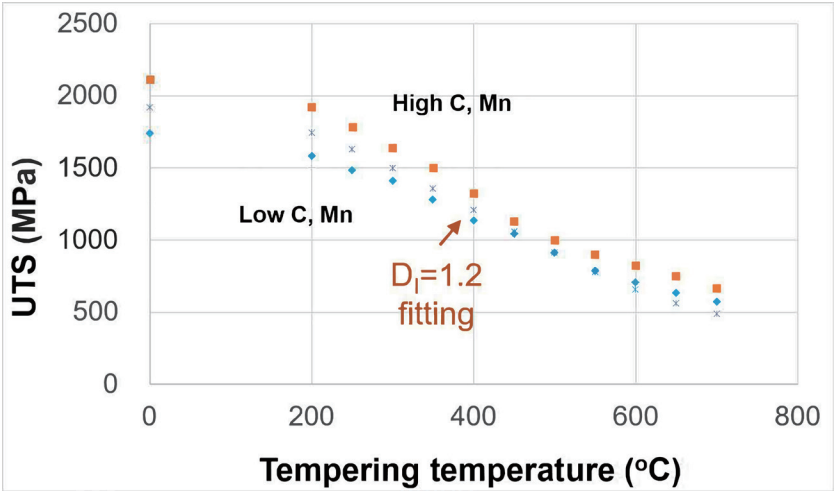

Fig. 8. (Color online) Tensile strength (UTS) fitting model of Q&T SAE 1038.

As shown in Figs. 7 and 8, the predicted values exhibit good agreement with experimental data, with coefficients of determination of $R^2 = 0.93$ for hardness and $R^2 = 0.91$ for UTS within the investigated tempering range. The maximum deviation remained within 5%, demonstrating the predictive capability of the sensing framework.

To illustrate practical applicability, a conceptual integration scheme for an intelligent production line is proposed. The sensing logic can be embedded into supervisory control and data acquisition (SCADA) systems or programmable logic controllers (PLCs) of heat treatment furnaces. Under such a configuration, D_I values and monitored thermal parameters may be used for in-process property estimation. If deviations in predicted as-quenched hardness are identified, the framework allows the calculation of appropriate tempering adjustments prior to final processing. This transition from post-process inspection to in-process estimation has the potential to reduce quality assurance latency and improve process consistency.

By leveraging the developed prediction equations for hardness and tensile strength, experimental data can be organized into a structured digital database, reducing experimental time and cost. The proposed framework also provides a foundation for future heat treatment expert systems and may support material selection and dimensional design at the product development stage.

4. Conclusions

A practical virtual sensor framework that enables the real-time estimation of mechanical properties in SAE 1038 steel was presented. The novelty of this framework lies in the incorporation of D_I as a material descriptor to normalize batch-to-batch variations within a

sensing-oriented architecture. The virtual sensor, established through dilatometry, Jominy testing, and mass effect analyses, demonstrated reliable predictive performance, with maximum prediction errors of less than 5% for both hardness and tensile strength. Furthermore, microstructural validation through SEM fractography supports the finding that the sensing logic reflects the transition from quasi-cleavage to microvoid coalescence with tempering. The conceptual implementation scenario further illustrates that this framework can be embedded into industrial control systems for in-process and real-time property estimation. Overall, this work provides a scalable framework for bridging metallurgical evolution with process control, contributing to real-time quality assurance and the advancement of intelligent heat treatment and self-sensing structural components.

References

1 M. Roessle and A. Fatemi: Int. J. Fatigue. **22** (2000) 495. https://doi.org/10.1016/S0142-1123(00)00026-8
2 G. Fett: ASM Handbook, Volume 4C: Induction Heat Treating and Heat Treatment (ASM International, Ohio, 2014) pp. 160–172.
3 L. Marroquin, L. Gómez, G. Calderón, G. Sosa, and E. Cruz: Appl. Mech. Mater. **13** (2008) 141. https://doi.org/10.4028/www.scientific.net/AMM.13-14.141
4 Z. Kaczkowski: Int. J. Appl. Electromagn. Mech. **5** (1994) 229. https://doi.org/10.1177/138354169400500309
5 L. Chen, P. Li, Y. Wen, and J. Qiu: J. Appl. Phys. **111** (2012) 07E503. https://doi.org/10.1063/1.3670607
6 R. Li, J. Liu, J. Xu, X. Ding, Y. Cheng, and Q. Liu: Processes **10** (2022) 1218. https://doi.org/10.3390/pr10061218
7 V. Savin, V. Kolesnikova, A. Ignatov, V. Zhukova, V. Rodionova, and A. Zhukov: Intermetallics **181** (2025) 108726. https://doi.org/10.1016/j.intermet.2025.108726
8 S. Santa-aho: Doctoral dissertation (Tampere University of Technology, Tampere, 2012).
9 P. Metaxas: Doctoral dissertation (University of Western Australia, Perth, 2009).
10 D. Rifai, A. Abdalla, K. Ali, and R. Razali: Sensors **16** (2016) 298. https://doi.org/10.3390/s16030298
11 E. Kirchner, T. Wallmersperger, T. Gwosch, J. Menning, J. Peters, R. Breimann, B. Kraus, P. Welzbacher, J. Küchenhof, D. Krause, E. Knoll, M. Otto, B. Muhammedi, S. Seltmann, A. Hasse, G. Schäfer, A. Lohrengel, S. Thielen, Y. Stiemcke, O. Koch, A. Ewert, T. Rosenlöcher, B. Schlecht, A. Prokopchuk, E. Henke, F. Herbst, S. Matthiesen, D. Riehl, F. Keil, K. Hofmann, F. Pape, D. Konopka, G. Poll, T. Steppeler, R. Ottermann, F. Dencker, M. Wurz, S. Puchtler, T. Baszenski, M. Winnertz, G. Jacobs, B. Lehmann, and K. Stahl: Adv. Sens. Res. **3** (2024) 2300113. https://doi.org/10.1002/adsr.202300113
12 J. Górka, W. Jamrozik, B. Wyględacz, M. Jamrozik, and B. Ferreira: Sensors **24** (2024) 3569. https://doi.org/10.3390/s24113569
13 E. Brinksmeier, D. Meyer, C. Heinzel, T. Lübben, J. Sölter, L. Langenhorst, F. Frerichs, J. Kämmler, E. Kohls, and S. Kuschel: Procedia CIRP. **71** (2018) 3. https://doi.org/10.1016/j.procir.2018.05.006
14 Z. Zhang, R. Qin, G. Li, Z. Liu, G. Wen, and W. He: IEEE Trans. Instrum. Meas. **71** (2022) 1. https://doi.org/10.1109/TIM.2021.3139653
15 ASTM A255, Standard Test Methods for Determining Hardenability of Steel.
16 ASTM E92, Standard Test Methods for Vickers Hardness and Knoop Hardness of Metallic Materials.
17 ASTM E18, Standard Test Methods for Rockwell Hardness of Metallic Materials.
18 ASTM E8/E8M, Standard Test Methods for Tension Testing of Metallic Materials.
19 M. Umemoto, N. Nishioka, and I. Tamura: J. Heat Treat. **2** (1981) 130. https://doi.org/10.1007/BF02833229
20 H. Burrier: ASM Handbook, Volume 1: Properties and Selection: Irons, Steels, and High-Performance Alloys (ASM International, Ohio, 1990) pp. 464–484.

About the Authors

Te-Kang Tsao received his B.S., M.S., and Ph.D. degrees in materials science and engineering from National Tsing Hua University (NTHU), Hsinchu, Taiwan, in 2010, 2012, and 2016, respectively. From 2017 to 2018, he served as a post-doc researcher at National Institute for Materials Science (NIMS) in Tsukuba, Japan. In 2018, he joined the Research & Development Division of China Steel Corporation (CSC), Kaohsiung, Taiwan, as a researcher. He is currently an assistant professor with the Department of Mechanical Engineering, National Kaohsiung University of Science and Technology (NKUST), Kaohsiung, Taiwan. He has authored more than 10 journal papers and holds eight patents. His research interests include steel product applications and high entropy alloys and materials processing technology. (tktsao@nkust.edu.tw)